

Purely Spectroscopic Determination of the Spin Hamiltonian Parameters in High-Spin Six-Coordinated Cobalt(II) Complexes with Large Zero-Field Splitting

Eugenii Ya. Misochko,^{*,†,‡} Alexander V. Akimov,[†] Denis V. Korchagin,^{†,‡} Joscha Nehr Korn,^{*,‡,§,||} Mykhaylo Ozerov,[‡] Andrew V. Paliu,^{†,||} Juan Modesto Clemente-Juan,^{†,||} and Sergey M. Aldoshin[†]

[†]Institute of Problems of Chemical Physics of RAS, Chernogolovka, Russia

[‡]National High Magnetic Field Laboratory & Florida State University, Tallahassee, Florida, United States

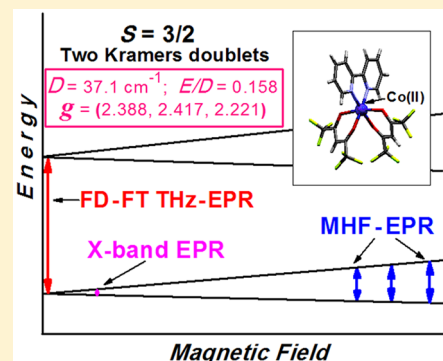
[§]Max Planck Institute for Chemical Energy Conversion, Mülheim/Ruhr, Germany

^{||}Institute of Applied Physics, Chisinau, Moldova

[†]Instituto de Ciencia Molecular, Universidad de Valencia, Paterna, Spain

Supporting Information

ABSTRACT: Accurate determination of the spin Hamiltonian parameters in transition-metal complexes with large zero-field splitting (ZFS) is an actual challenge in studying magnetic and spectroscopic properties of high-spin transition metal complexes. Recent critical papers have convincingly shown that previous determinations of these parameters, based only on the magnetic data, have low accuracy and reliability. A combination of X-band electron paramagnetic resonance (EPR) spectroscopy and SQUID magnetometry seems to be a more convincing and accurate approach. However, even in this case, the accuracy of the determination of the spin Hamiltonian parameters is strongly limited. In this work, we propose a purely spectroscopic approach, in which three complementary EPR spectroscopic techniques are used to unambiguously with high accuracy determine the spin Hamiltonian parameters for transition-metal complexes with $S = 3/2$. The applicability of this approach is demonstrated by analyzing the new quasi-octahedral high-spin Co(II) complex $[\text{Co}(\text{hfac})_2(\text{bpy})]$ (I). Along with the conventional X-band EPR spectroscopy, we also use such advanced techniques as multi-high-frequency EPR spectroscopy (MHF-EPR) and frequency-domain Fourier-transform THz-EPR (FD-FT THz-EPR). We demonstrate that the experimental data derived from the X-band and MHF-EPR EPR spectra allow determination of the g tensor ($g_x = 2.388$, $g_y = 2.417$, $g_z = 2.221$) and the ZFS rhombicity parameter $E/D = 0.158$. The axial ZFS parameter $D = 37.1 \text{ cm}^{-1}$ is measured for I with the aid of FD-FT THz-EPR spectroscopy, which is able to detect the high-energy EPR transition between the two Kramers doublets. CASSCF/NEVPT2 quantum-chemical calculations of magnetic parameters and magnetic direct current (dc) measurements are performed as well as testing options, and the results obtained in these ways are in good agreement with those derived using the proposed spectroscopic approach.



I. INTRODUCTION

Mononuclear transition-metal complexes, exhibiting slow magnetic relaxation, are known as single-ion magnets (SIMs). These complexes represent an important class of single-molecule magnets (SMMs) which are of current interest in molecular magnetism due to their intriguing physical properties (e.g., magnetic bistability at low temperatures, quantum tunneling of magnetization, etc.) and promising applications.^{1–9}

SMMs including SIMs are usually characterized by a large axial zero field splitting (ZFS) that represents the main anisotropic contribution to the spin Hamiltonian. The latter also includes the rhombic ZFS contribution as well as the anisotropic Zeeman term defined by the g tensor. The knowledge of the parameters of the spin Hamiltonian is of crucial importance because just these parameters define the

character and strength of the magnetic anisotropy and hence the SIM properties of the complexes. However, direct experimental determination of these parameters for transition-metal complexes with large ZFS is far from trivial. Earlier^{10,11} and more recent^{8,12,13} reviews discuss this issue.

The most widely used approach for the determination of ZFS and g tensors is based on SQUID measurements of the direct current (dc) magnetic properties, such as the temperature dependence of the magnetic susceptibility at low dc field and field dependences of magnetization at various temperatures. SQUID magnetometry is relatively simple and broadly available; however, it has significant drawbacks. One such drawback is related to a rather large number of unknown

Received: July 23, 2019

Published: November 21, 2019

parameters in the spin Hamiltonian, which often results in overparametrization in the course of fitting the magnetic dc data. Another drawback is that the magnetic dc properties measured for a polycrystalline sample often have low sensitivity to the sign of the axial ZFS parameter D and to the magnitude of the rhombic ZFS parameter E . In addition, these properties are only weakly dependent on the anisotropy of the g tensor. Therefore, an approach based solely on the analysis of the dc magnetic data has low accuracy and sometimes gives an erroneous conclusion about the character of the magnetic anisotropy.^{8,10,11,13}

A more accurate and precise method to measure ZFS parameters and g tensor is provided by EPR spectroscopy. The capabilities of EPR spectroscopy for such purposes strongly depend on the ratio between the radiation energy quantum $h\nu$ and the magnitude of D . The optimal condition is $h\nu \gtrsim |D|$. Since many transition-metal complexes have sizable magnitudes of D up to 100 cm^{-1} (e.g., in Co(II)-based SIMs values of D ranging from 5 to 129 cm^{-1} have been found^{14–22}), the usefulness of the conventional X-, Q-, and W-band EPR spectroscopy ($h\nu \approx 0.3, 1.2,$ and 3 cm^{-1} , respectively) is strongly constrained. For this reason, previously developed advanced spectroscopic techniques,^{23–30} operating in the higher frequency range, such as multi-high-frequency EPR (MHF-EPR) ($2.3 \text{ cm}^{-1} < h\nu < 17.1 \text{ cm}^{-1}$)^{13,31} and frequency-domain Fourier-transform THz-EPR (FD-FT THz-EPR) ($4 \text{ cm}^{-1} < h\nu < 250 \text{ cm}^{-1}$)^{13,32,33} have been applied in recent years. Unfortunately, no single universal method for determining all parameters for all cases exists. For this reason, recent efforts have been aimed at the development of a combined approach which takes the best from various experimental techniques. For example, a combination of NMR with FD-FT THz-EPR³⁴ and of NMR with MHF-EPR³⁵ has been applied.

Among numerous 3d metal complexes showing SIM behavior, those based on high-spin Co(II) complexes with quasi-octahedral coordination of the Co ion are especially interesting because unlike conventional SMMs and SIMs they often exhibit slow magnetic relaxation for both easy-plane and easy-axis types of magnetic anisotropy.^{14,36–48} This atypical behavior was shown to be a result of the Kramers character of the Co(II) ion.⁵

Here we report the synthesis of the six-coordinated Co(II) complex $[\text{Co}(\text{hfac})_2(\text{bpy})]$ (I) with two hexafluoroacetylacetonate (hfac) ligands and one 2,2'-dipyridyl ligand (bpy). However, this article is focused on presenting a new combined spectroscopic approach to determine the full set of spin Hamiltonian parameters, and I is merely an example for our method. Along with conventional X-band EPR spectroscopy, we apply advanced techniques such as MHF-EPR and FD-FT THz-EPR. Since the axial ZFS parameter D for this complex has a sizable magnitude, the FD-FT THz-EPR measurements play a key role in the unambiguous and accurate determination of the spin Hamiltonian parameters. It is worth noting that the applicability of the spin Hamiltonian for the description of the magnetic and spectroscopic properties of the quasi-octahedral Co(II) complexes is not a priori clear because of the existence of the unquenched orbital angular momentum, and so it requires special justification. In order to prove the validity of the spin Hamiltonian formalism for complex I, we performed multiconfigurational ab initio calculations of the energy levels. In this way, we have demonstrated that the description based on the spin Hamiltonian is adequate in the present case, and also we have evaluated the spin Hamiltonian parameters for

complex I. In addition, dc magnetic measurements have been performed in order to explore to what extent the magnetic data are consistent with the spectroscopic data.

Finally, we argue that the applicability of the proposed self-consistent spectroscopic approach is not restricted to the case of high-spin Co(II) complexes in different coordination environments but can also be used for the characterization of other 3d metal complexes with $S = 3/2$, provided that the spin Hamiltonian is applicable.

II. EXPERIMENTAL SECTION

II.A. Synthesis and Characterization of $[\text{Co}(\text{hfac})_2 \text{bpy}]$ (I) and Its Magnetically Diluted Analogue. All chemicals were purchased from commercial sources and used without further purification. Elemental analysis was performed on a Vario MICRO Cube analyzer. The IR spectra of microcrystalline powders were recorded on a Bruker Alpha FT-IR spectrometer using attenuated total reflection accessory. The powder XRD patterns were recorded at room temperature on an ARL X'TRA X-ray diffractometer.

Complex I was prepared by adding 0.5 mmol of bpy dissolved in 2.5 mL of EtOH to 2.5 mL of an EtOH solution of 0.5 mmol $[\text{Co}(\text{hfac})_2(\text{H}_2\text{O})_2]$ at room temperature. The obtained bright orange precipitate was filtered off and washed with cold EtOH and ether. Single crystals of complex I, suitable for X-ray diffraction, were obtained by recrystallization from a mixture of dichloromethane and EtOH (1/1). A magnetically diluted sample for X-band EPR spectroscopy, $[\text{Co}_{0.02}\text{Zn}_{0.98}(\text{hfac})_2 \text{bpy}]$ (II), was prepared by cocrystallization of complex I and its isostructural Zn analogue with ratio Co/Zn = 1/50 in warm dichloromethane solution (see the Supporting Information for details).

The powder XRD measurements showed that samples are monophasic crystalline materials (Figure S1).

II.B. Single-Crystal X-ray Analysis. X-ray data for a single crystal of I were collected on a Agilent XCalibur CCD diffractometer with EOS detector (Agilent Technologies UK Ltd., Yarnton, Oxfordshire, England). The recording of reflections and the determination and refinement of unit cell parameters were performed at 100.0(1) K with monochromatic Mo $K\alpha$ radiation ($\lambda = 0.71073 \text{ \AA}$), using the CrysAlis PRO software.⁴⁹ The structure was solved by direct methods and refined against all F^2 data. All non-hydrogen atoms were refined with anisotropic thermal parameters, and positions of hydrogen atoms were obtained from difference Fourier syntheses and refined with riding model constraints. All calculations were performed with the SHELXTL software.⁵⁰ The X-ray crystal structure data have been deposited with the Cambridge Crystallographic Data Center, with reference code CCDC 1911055. Selected crystallographic parameters and the data collection and refinement statistics are given in Table S1.

II.C. CW X-band EPR Spectroscopy. EPR spectra were measured with a Bruker Elexys E500 spectrometer working in the X-band (9.5 GHz). Magnetically diluted powder samples II were placed in a 2 mm diameter quartz tube, which was pumped out and filled with helium to obtain rapid thermal stabilization of the entire sample at low temperatures. An RTI ESRcryo202 continuous flow cryostat refrigerated with liquid helium was used for cooling the samples up to 4.2 K. The modulation amplitude (10 G at 100 kHz) and microwave power (6.325 mW) were low enough to avoid line broadening and saturation effects.

II.D. Multi-High-Frequency EPR Spectroscopy. MHF-EPR data were collected using a transmission-type spectrometer at the National High Magnetic Field Laboratory (NHMFL), Tallahassee, FL, USA.⁵¹ Frequencies in the range of 50–650 GHz were generated by a phase-locked microwave source combined with several multipliers (all from Virginia Diodes). Sample temperatures from 5 to 50 K were reached using a lHe flow cryostat. Magnetic fields of up to 14.5 T were obtained by using a superconducting magnet (Oxford Instruments). Samples of I and II were finely ground and placed in a PE cup with a Teflon stopper.

II.E. Frequency-Domain Fourier-Transform THz-EPR. FD-FT THz-EPR experiments were conducted at the NHMFL.²⁵ Briefly, the

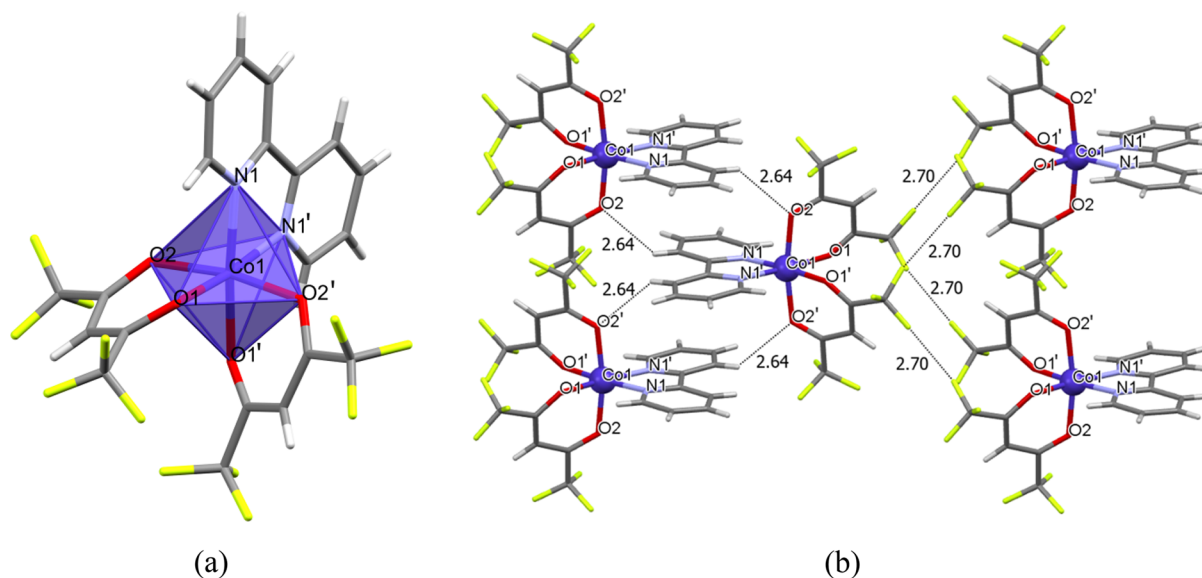


Figure 1. (a) Molecular structure of complex I. (b) Fragment of the crystal structure of I. Color code: gray, C; light green, F; white, H. Dashed lines show intermolecular contacts (distances in Å).

unpolarized radiation of an Hg arc lamp is passed through an FT-IR spectrometer (Bruker Vertex 80v), focused on the sample, and detected by a Si bolometer (Infrared Laboratory). Both the sample and the bolometer are in thermal equilibrium with a lHe bath of a 17 T superconducting optical magnet. The sample (a few milligrams of I mixed with eicosane fixed with Scotch tape to fill an aperture completely) is placed in the field center of that magnet, while the bolometer is slightly away from it. As in traditional FT-IR spectroscopy a reference is required. However, the strong non-magnetic absorption does not allow use of a blank. Hence, spectra recorded at different magnetic fields are divided. Details on how to understand such magnetic field division spectra (MDS) can be found in ref 52. Here MDS for the magnetic field value B_0 is obtained by division of the spectrum measured at B_0 by a spectrum measured at $B_0 + 1$ T. Spectra were measured with a scanner velocity of 5 kHz and an experimental resolution of 0.8 cm^{-1} . At each field value three measurements for 4 min each were performed.

II.F. EPR Simulations. All EPR simulations and fitting procedures were done using the EasySpin program package for Matlab.⁵³ A recently developed extension of EasySpin was used for simulations of FD-FT THz-EPR spectra.^{54,55}

II.G. dc Magnetic Measurements. dc magnetic properties were measured with a SQUID magnetometer (MPMS-5XL, Quantum Design). Magnetic susceptibility was measured in the temperature range 2–300 K with an applied field of $B = 0.1$ T. Diamagnetic corrections were made using the Pascal constants.⁵⁶ Isothermal magnetization curves have been measured at temperatures $T = 2, 3, 4, 5, 7, 10$ K.

II.H. Quantum Chemical Calculations. Quantum chemical calculations of ZFS parameters and g tensors were performed based on state-averaged complete-active-space self-consistent-field (SA-CASSCF) wave functions complemented by N -electron valence second-order perturbation theory (NEVPT2)^{57–61} using the ORCA program package.⁶² The active space of the CASSCF calculations was composed of 7 electrons in 5 d orbitals of a Co atom: CAS(7,5). The state-averaged approach was used, in which all 10 quartet and 40 doublets states were averaged with equal weights. The polarized triple- ζ -quality basis set def2-TZVP was used for cobalt, oxygen, and nitrogen atoms, while the def2-SVP basis set was used for other atoms.^{63–65} The calculations were performed with the geometry of the experimentally determined X-ray structure. The ZFS parameters were calculated on the effective Hamiltonian theory,⁶⁶ in which an approximation to the Breit–Pauli form of the spin–orbit coupling operator (SOMF approximation)⁶⁷ was utilized. The g tensor for a

pseudo-spin $S' = 1/2$ state has been calculated using the quasi-degenerate perturbation theory (QDPT) approach within an individual Kramers doublet.⁶⁸ Splitting of the d orbitals was analyzed within the ab initio ligand field theory (AILFT)^{69,70} as implemented in ORCA software.

III. RESULTS AND DISCUSSION

III.A. Molecular and Crystal Structure. Compound I crystallizes in the monoclinic space group $C2/c$. Figure 1a shows the molecular structure of complex I. The cobalt(II) ion is located on the second-order rotational axis. This ion is coordinated by two hexafluoroacetylacetonate ligands and one 2,2'-dipyridyl ligand. The Co(II) ion has a distorted-pseudo-octahedral coordination environment with X–Co–X angles of bidentate ligands less than 90° (for O(1)–Co–O(2) $86.20(7)^\circ$ and N(1)–Co–N(1') $77.9(1)^\circ$). The bond angles O(2)–Co–O(2') and O(1)–Co–N(1) are not linear ($169.7(1)^\circ$ and $174.50(7)^\circ$, respectively). The bond lengths Co–O(1) $2.061(2)$ Å and Co–O(2) $2.075(2)$ Å differ insignificantly, and the length of the Co–N(1) bond is $2.097(2)$ Å. The dihedral angle between the pyridine rings is 7.6° : i.e., the 2,2'-dipyridyl ligand is not planar.

In general, the molecular structure of complex I is similar to structures of analogous complexes with acetylacetonate^{71,72} or substituent bipyridyl ligands.⁷³ At the same time, the replacement of methyl and trifluoromethyl groups with a *tert*-butyl moiety in the β -diketonate ligands leads to a greater deviation of Co(II) ion coordination from ideal octahedral, apparently due to steric effects.⁷⁴

In the crystal packing, Co(II) ions are well-shielded from each other with an interatomic separation that is longer than 7.8 Å, thus excluding significant intermolecular magnetic interactions. In general, the crystal structure of complex I is stabilized by weak van der Waals contacts O...H–C and shortened contacts F...F ≈ 2.70 Å (Figure 1b).

III.B. Zeeman Energy Levels and EPR Transitions for Mononuclear Spin $S = 3/2$. The question about the applicability of a spin Hamiltonian to the description of high-spin Co(II) complexes is not in general trivial and requires justification in each particular case. In fact, the ground

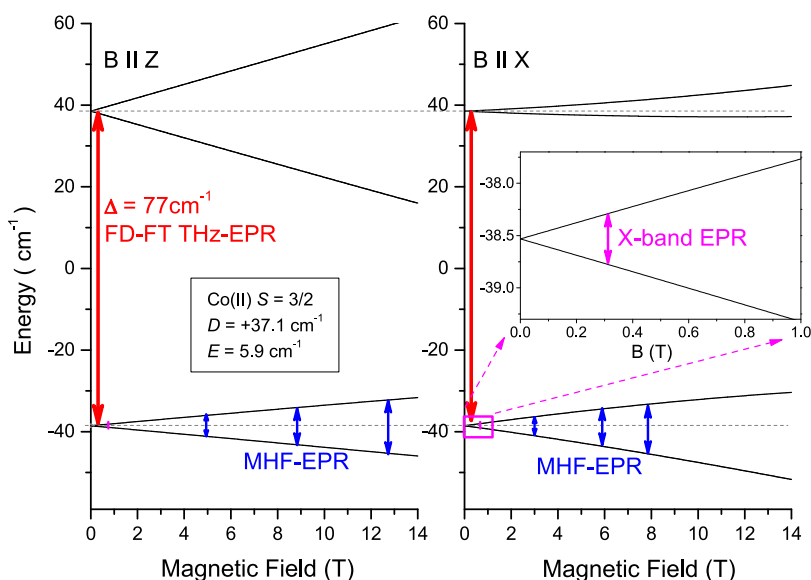


Figure 2. Zeeman energy levels for a spin quartet with ZFS parameters $D = 37.1 \text{ cm}^{-1}$ and $\eta = E/D = 0.158$ simulated from eq 1 with $\mathbf{g} = (2.388, 2.417, 2.221)$. The magenta and blue vertical bars indicate the allowed X-band and MHF EPR transitions within the low-lying Kramers doublet with the effective spin projections $M_s = \pm 1/2$. The red vertical bar indicates the FD-FT THz-EPR transition between the two Kramers doublets with the energy gap Δ .

4T_1 term of an octahedrally coordinated Co(II) ion possesses not only spin but also unquenched orbital angular momentum. For this reason, a Griffith Hamiltonian which explicitly takes into account the orbital angular momentum is often used for the adequate description of such cobalt complexes. (see the Supporting Information for details). However, as was shown by numerous authors (see for example^{14,47,75–79}) the Hamiltonian to describe low-energy magnetic properties can often be reduced to a spin Hamiltonian, which is much more simple and convenient for the analysis of the magnetic data and EPR spectra. Below (see section III.G) we will demonstrate that in the present case the low-lying energy levels obtained with the aid of CASSCF/NEVPT2 quantum chemical calculations are consistent with the eigenvalues of the spin Hamiltonian, thus justifying the applicability of this Hamiltonian.

Accordingly, the spectroscopic properties of complexes I and II have been analyzed applying the following spin Hamiltonian for $S = 3/2$:

$$\begin{aligned}
 H &= \beta \mathbf{B} \mathbf{g} \mathbf{S} + \mathbf{S} \mathbf{D} \mathbf{S} + \mathbf{S} \mathbf{A} \mathbf{I} \\
 &= \beta (g_z B_z S_z + g_x B_x S_x + g_y B_y S_y) + D \left[S_z^2 - \frac{1}{3} S(S+1) \right] \\
 &\quad + E(S_x^2 - S_y^2) + A_z S_z I_z + A_x S_x I_x + A_y S_y I_y, \quad (1)
 \end{aligned}$$

where \mathbf{g} is the electronic \mathbf{g} tensor with principal values g_x , g_y , and g_z , \mathbf{D} is the ZFS tensor defined (up to second order) by the axial ZFS parameter D and rhombic ZFS parameter E , \mathbf{A} is the tensor with the principal values A_x , A_y , and A_z describing the hyperfine interaction between the electronic spin $S = 3/2$ and the spin $I = 7/2$ of the cobalt nucleus, \mathbf{B} is the dc magnetic field, β is the Bohr magneton, and finally S_z , S_x , S_y , and I_z , I_x , I_y are the components of the electronic spin 3/2 operator and nuclear spin 7/2 operator, respectively.

The ZFS parameters D and E in the Hamiltonian of eq 1 are obtained with the aid of the following conventional definitions:

$$D = \frac{3}{2} D_{zz} \quad E = \frac{D_{xx} - D_{yy}}{2} \quad (2)$$

where D_{xx} , D_{yy} , and D_{zz} are the principal values of the ZFS tensor.

The ZFS term causes splitting of the quartet ground state into two Kramers doublets separated by the energy gap (see Figure 2)

$$\Delta = 2D\sqrt{1 + 3\eta^2} \quad (3)$$

where $\eta = E/D$ is the rhombicity parameter. In the axial case ($\eta = 0$) these Kramers doublets are characterized by the effective spin projections: $M_s = \pm 3/2$ and $M_s = \pm 1/2$, where the latter is the ground state for $D > 0$.⁸⁰ Provided that the energy gap between the ground and first excited Kramers doublets considerably exceeds the Zeeman splitting of these doublets, one can describe the ground Kramers doublet by the following effective pseudospin 1/2 Hamiltonian which includes the Zeeman term and the hyperfine interaction of pseudospin $S' = 1/2$ with the $I = 7/2$ cobalt nucleus:

$$H = \beta \mathbf{B} \mathbf{g}' \mathbf{S}' + \mathbf{S}' \mathbf{A}' \mathbf{I} \quad (4)$$

where \mathbf{S}' is the pseudo spin 1/2 operator and \mathbf{g}' and \mathbf{A}' are the effective \mathbf{g} and hyperfine tensors defined in the principal axis system which is assumed to be common for both of these tensors. Since the pseudo spin 1/2 Hamiltonian represents the projection of the full spin 3/2 Hamiltonian (eq 1) onto the truncated space of the ground Kramers doublets, the parameters involved in the effective Hamiltonian, eq 4, prove to be dependent on the parameters of the spin 3/2 Hamiltonian. This point, which is important for our consideration, will be discussed below (see section III.F).

At low temperatures, i.e. $\Delta \gg kT$, only the doublet lowest in energy is thermally populated. Therefore, the X-band spectrum contains the EPR transitions within this doublet. Direct measurements of the large ZFS require very high excitation frequencies. Thus, we applied FD-FT THz-EPR spectroscopy.

Experiments at zero magnetic field allow direct determination of the energy gap Δ , as shown in Figure 2.

III.C. X-band EPR Spectra. The X-band EPR spectrum of magnetically diluted sample II, $[\text{Co}_{0.02}\text{Zn}_{0.98}(\text{hfac})_2\text{bpy}]$, measured at 5 K is shown in Figure 3a. The spectrum consists

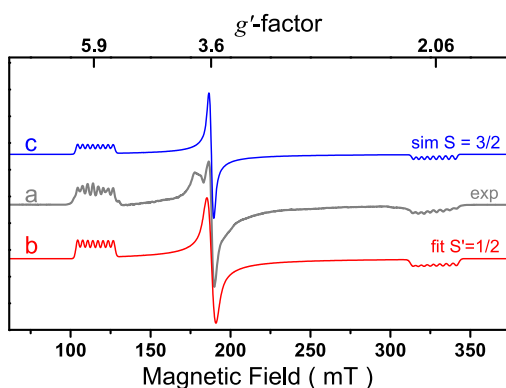


Figure 3. (a) Powder X-band EPR spectrum of magnetically diluted sample II $[\text{Co}_{0.02}\text{Zn}_{0.98}(\text{hfac})_2\text{bpy}]$ measured at 5 K. (b) Fitted powder spectrum for the effective pseudo spin 1/2 Hamiltonian (eq 4) with the effective magnetic parameters $g'_1 = 2.063$, $g'_2 = 3.599$, $g'_3 = 5.854$ and $A'_1 = 108$ MHz, $A'_2 = 10$ MHz, $A'_3 = 260$ MHz. (c) Simulated powder spectrum for the spin Hamiltonian eq 1, with the parameters $D = 37.1$ cm^{-1} , $\eta = 0.158$, $g_x = 2.388$, $g_y = 2.417$, $g_z = 2.221$, $A_x = 6.6$ MHz, $A_y = 107$ MHz, and $A_z = 116$ MHz.

of three intense lines at 120, 180, and 330 mT. The low-field and high-field EPR lines contain the resolved hyperfine structure appearing due to interaction with the magnetic $I = 7/2$ cobalt nucleus. The recorded spectrum is a typical spectrum for high-spin Co(II) complexes with $S = 3/2$ and a positive sign of the axial ZFS parameter D .^{14,47,13,81} We fitted the X-band EPR spectrum using the effective pseudo spin 1/2 Hamiltonian (eq 4) and obtained $g'_1 = 2.063(3)$, $g'_2 = 3.599(3)$, $g'_3 = 5.854(6)$ and $A'_1 = 108(5)$ MHz, $A'_2 = 10(5)$ MHz, $A'_3 = 260(5)$ MHz. The simulated spectrum with the best fitted parameters is shown in Figure 3b. A potential rationale for the observed additional lines can be found in the Supporting Information.

III.D. Multi-High-Frequency EPR Spectra. The variable-frequency MHF-EPR spectra of I, measured at 5 K, are shown in Figure 4. In addition to small signals due to the unavoidable presence of solid oxygen,⁸² three resonances were observed at frequencies of 68–392 GHz. At the highest measured frequency of 513 GHz only two resonances were observed. According to eq 4, the resonance condition is $h\nu = \beta g'_i(v) B_i^{\text{res}}(v)$, where g'_i is the effective g factor to the i th resonance observed at a magnetic field of B_i^{res} measured with the microwave frequency ν , and h is the Planck constant. Thus, it was found that the three observed resonances are almost frequency independent (see Figure 5) and are close to the values obtained at X band. The resonance g'_i was not observed at 513 GHz, as it corresponds to a field value not accessible with the used superconducting magnet. The observed resonances were quite broad. As dipolar interactions between Co(II) atoms in adjacent molecules are expected to have a significant influence on the line width, we also investigated the magnetically diluted complex II (see Figure S4). Indeed, an improved line width was observed. However, the signal to noise was significantly reduced, essentially outweighing the improvements. In any event, the obtained g' values were

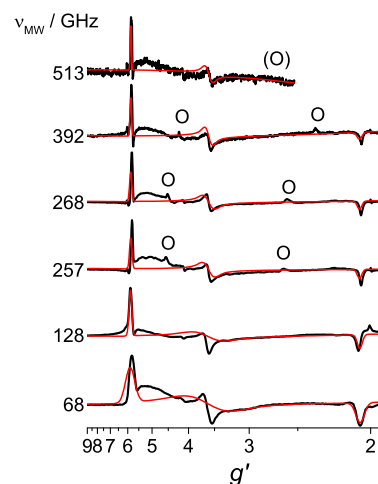


Figure 4. Powder MHF-EPR spectra of I measured at $T = 5$ K and at the indicated frequencies. The abscissa axis shows the effective g' value. Experimental data are rescaled for each frequency individually. Experimental data are shown in black. Signals due to solid oxygen are marked with an O. Simulations with the spin Hamiltonian eq 4 with the effective magnetic parameters $g'_1 = 2.063$, $g'_2 = 3.599$, and $g'_3 = 5.854$ are shown in red.

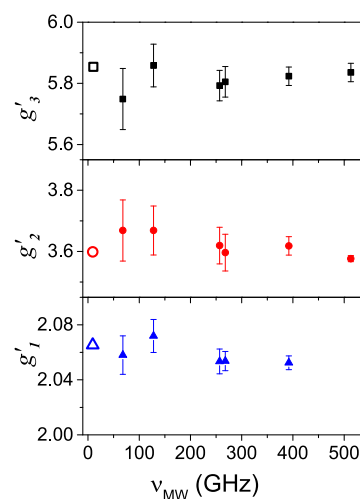


Figure 5. Effective g factors derived from field domain EPR experiments: i.e., X-band (hollow symbols) and MHF-EPR (filled symbols).

virtually identical for I and II, indicating that dilution had a minor influence on the magnetic properties. Experiments on I at various temperatures reveal a decreasing signal intensity with increasing temperature (see Figure S5). This further corroborates the assignment of the EPR lines to transitions involving the ground state.

III.E. Frequency-Domain Fourier-Transform THz-EPR Spectra. The measured FD-FT THz-EPR spectra are shown as MDS in Figure 6 (a contour plot is shown in Figure S6). In the $B_0 = 0$ T spectrum a pronounced minimum was observed at 77 cm^{-1} . At both lower and higher energies it is surrounded by maxima. The maximum at lower energies shifts to lower energies and broadens beyond recognition around 4 T. The field dependence of the minimum and the maximum at higher energies is hard to follow, as in these regions several features with fluctuating intensity but unaltered energy were observed. Due to the fact that their energies are not affected by a

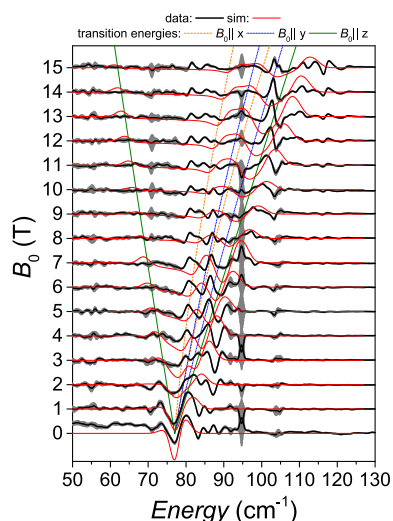


Figure 6. Experimental FD-FT THz-EPR spectra of I shown as MDS (black lines) measured at the indicated magnetic fields. The gray shaded area indicates an uncertainty estimate based on the standard deviation of the four measured subspectra. Simulations with eq 1 and $D = 37.13 \text{ cm}^{-1}$, $\eta = 0.158$, and $\mathbf{g} = (2.388, 2.417, 2.221)$ are shown as red lines. Transition energies for magnetic fields applied along the principal axis are shown as dashed orange (x), dotted blue (y) and solid green (z) lines.

magnetic field, we assigned them to be nonmagnetic. However, especially at higher fields, a broad maximum shifting to higher energies with an increasing magnetic field can be identified. Hence, we assign the observed minimum to the ZFS splitting and therefore experimentally observed $\Delta = 77(1) \text{ cm}^{-1}$. It is generally hard to determine the rhombicity η and \mathbf{g} values from FD-FT THz-EPR experiments. Due to the strong distortion observed here, it is outright impossible for I.

III.F. Magnetic Parameters of the Complex under Study. The spin Hamiltonian eq 1 contains five magnetic parameters: namely, g_x , g_y , g_z , D , and η . From the X-band EPR and MHF-EPR experiments we obtained effective g' values: $g'_1 = 2.063$, $g'_2 = 3.599$, and $g'_3 = 5.854$. Further, we have obtained $\Delta = 77 \text{ cm}^{-1}$ from FD-FT THz-EPR. Here, we will demonstrate how the magnetic parameters can be determined from these experimental results. The effective g' values can be directly related to the \mathbf{g} values in eq 1. For a positive D value and under the assumption of collinear \mathbf{D} , \mathbf{g} , and \mathbf{g}' tensors they are^{5,83,84}

$$\frac{g'_x}{g_x} = 1 + \frac{1 - 3\eta}{\sqrt{1 + 3\eta^2}} \quad (5a)$$

$$\frac{g'_y}{g_y} = 1 + \frac{1 + 3\eta}{\sqrt{1 + 3\eta^2}} \quad (5b)$$

$$\frac{g'_z}{g_z} = \frac{2}{\sqrt{1 + 3\eta^2}} - 1 \quad (5c)$$

It should be emphasized that the observed \mathbf{g}' values are not yet assigned to the principal directions. For this reason, we have calculated \mathbf{g} values as a function of $\eta = E/D$ for all six possible assignments. These six assignments are as follows: $(g'_x, g'_y, g'_z) \leftrightarrow (g'_1, g'_2, g'_3)$ or (g'_1, g'_3, g'_2) or (g'_2, g'_1, g'_3) or (g'_2, g'_3, g'_1) or (g'_3, g'_1, g'_2) or (g'_3, g'_2, g'_1) . On the basis of the literature, realistic \mathbf{g} values for pseudo-octahedral high-spin Co(II) are in

the range of approximately 2–3.^{14,16} Inspecting the results (see Figure S7), we have found completely unrealistic \mathbf{g} values for all assignments with the exception of the assignment $(g'_x, g'_y, g'_z) \leftrightarrow (g'_2, g'_3, g'_1)$ that will be adopted at this step. As a next step we will correlate the anisotropy of the \mathbf{g} and \mathbf{D} tensors. Assuming that spin–orbit coupling is the main reason for ZFS and Russell–Saunders coupling is strictly valid, the following relation applies:⁵

$$\eta(\mathbf{g}) = \frac{g_x - g_y}{g_z - (g_x + g_y)/2} \quad (6)$$

In theory, both anisotropies should be equal: $\eta(\mathbf{g}) = \eta(\mathbf{D})$. Hence, with the use of eqs 5a–5c and eq 6 we get

$$f(\eta) = \frac{g_x(\eta) - g_y(\eta)}{g_z(\eta) - [g_x(\eta) + g_y(\eta)]/2} - \eta \quad (7)$$

A graphical solution for $f(\eta) = 0$ is shown in Figure 7A. Indeed, only for the combination $(g'_x, g'_y, g'_z) \leftrightarrow (g'_2, g'_3, g'_1)$ with $\eta =$

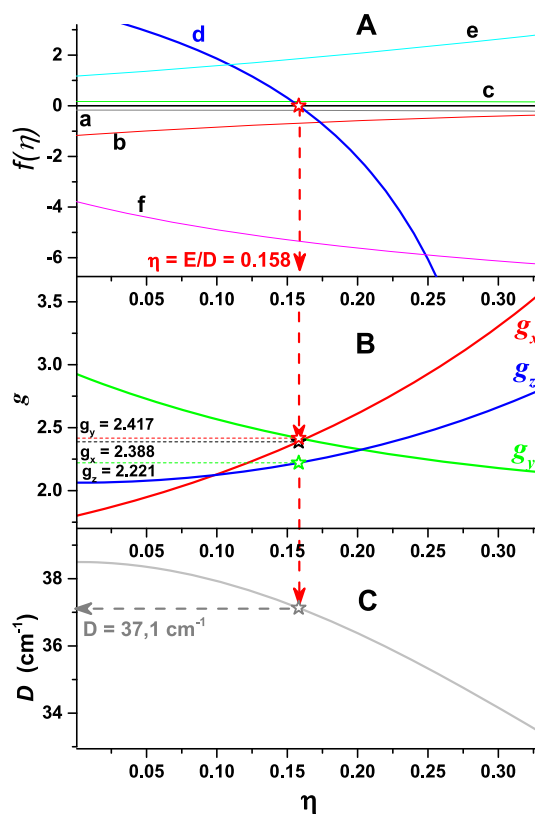


Figure 7. (A) Dependences $f(\eta)$ plotted for all possible assignments $(g'_x, g'_y, g'_z) \leftrightarrow$ (a) (g'_1, g'_2, g'_3) , (b) (g'_1, g'_3, g'_2) , (c) (g'_2, g'_1, g'_3) , (d) (g'_2, g'_3, g'_1) , (e) (g'_3, g'_1, g'_2) , (f) (g'_3, g'_2, g'_1) . The intersection of this function with the ordinate $y = 0$ at $\eta = 0.158(1)$ is highlighted by a star. (B) Principal \mathbf{g} values (g_x red; g_y green; g_z blue) as a function of η for $(g'_x, g'_y, g'_z) \leftrightarrow (g'_2, g'_3, g'_1)$. (C) Magnitude of D as a function of η from eq 3.

$0.158(1)$ can a solution be obtained. Subsequently, $g_x = 2.388(3)$, $g_y = 2.417(3)$, $g_z = 2.221(3)$ (see Figure 7B) and $D = 37.1(6) \text{ cm}^{-1}$ (see Figure 7C) are determined with the help of eqs 5a–5c and eq 3, respectively. Finally, the principal values of the hyperfine interaction tensor \mathbf{A} are straightforwardly determined using the relations $A_i/A'_i = g_i/g'_i$ ($i = x, y, z$) as A_x

= 7(1) MHz, A_y = 107(1) MHz, and A_z = 116(1) MHz. Simulations with eq 1 and these parameters are shown in Figures 3 and 6. As a last check, we performed similar calculations under the assumption of a negative D value (see the Supporting Information). No reasonable parameter set could be identified, further strengthening the assignment of D to a positive value.

III.G. Quantum Chemical Calculations. The CASSCF(7,5)/NEVPT2 computed low-lying spin-free (δ_E) and spin-orbit states (Δ_E) energies are given in Table 1. In addition we

Table 1. CASSCF(7,5)/NEVPT2 Computed Low-Lying Spin-Free (δ_E) and Spin-Orbit States (Δ_E) Energies (cm^{-1}) for **I along with the Inferred Symmetry Label for Idealized D_{4h} Symmetry**

term	spin-free state (δ_E)	spin	spin-orbit state (Δ_E)
${}^4A_{2g}$	0	3/2	0
			101
4E_g	1081	3/2	1118
			1316
	1562	3/2	1820
			1910

inferred the symmetry labels for an idealized D_{4h} symmetry. The six spin-orbit states lowest in energy (Kramers doublets) roughly correspond to the Griffith diagram¹⁴ at a large positive value of the axial crystal field parameter, thus showing that the spin Hamiltonian description used is an adequate one. Spin-orbit coupling results in the first excited Kramers doublet being located 101 cm^{-1} above the ground state (Table 1). This is just the energy gap, which is determined from the experiment as $\Delta = 77(1) \text{ cm}^{-1}$. As the energy difference to the next higher levels is more than 1000 cm^{-1} , the spin Hamiltonian can be used.

The results of our CASSCF/NEVPT2 quantum chemical calculations of magnetic parameters for the studied complex **I** are presented in Table 2. The calculated parameters for all

Table 2. CASSCF/NEVPT2 Quantum Chemical Calculated and Experimental Magnetic Parameters of Complex **I**

param	calcd/(exptl)	
	full spin Hamiltonian, eq 1, for $S = 3/2$	effective pseudo spin 1/2 Hamiltonian, eq 4
g_x	2.406/(2.388)	3.408/(3.599)
g_y	2.572/(2.417)	6.354/(5.854)
g_z	2.059/(2.221)	1.999/(2.063)
g_{iso}	2.346/(2.342)	3.92/(3.84)
$D, \text{ cm}^{-1}$	48.2/(37.1)	
η	0.181/(0.158)	

three tensors, \mathbf{g} , \mathbf{g}_{eff} and \mathbf{D} , somewhat agree with the experimental data. More importantly, the calculation results support the following conclusions from the analysis of the experimental data: (i) the sign of parameter D is positive, (ii) the principal axes orientations of all three tensors coincide, (iii) the assignment of g'_x, g'_y and g'_z with respect to the g'_1, g'_2 and g'_3 values corresponds to that accepted above in the section II, namely $(g'_x, g'_y, g'_z) \leftrightarrow (g'_2, g'_3, g'_1)$ (see Figure S2), and (iv) spin-orbit coupling is the main source of magnetic anisotropy in the \mathbf{g} and \mathbf{D} tensors: in fact, the spin-spin coupling contribution to the \mathbf{D} tensor of complex **I** is equal to

0.78 cm^{-1} , which is only $\sim 2\%$ of the total D parameter. The ground spin-free state is an orbital singlet (${}^4A_{2g}$ state in the case of idealized D_{4h} symmetry), while the two excited levels show the rhombic splitting of the 4E_g term, as can be seen in the calculated orbital scheme in Figure S10 and Table S2. This configuration of states straightforwardly rationalizes the positive D value.^{14,47}

Splitting of the d orbitals has been analyzed within the ab initio ligand field theory (AILFT).^{69,70} AILFT analysis shows that the scheme of the d orbitals is close to the scheme peculiar to quasi-octahedral coordination (see energy diagram and shapes of corresponding one-electron LFT states in Figure S10 and also the relative energies and composition of one-electron states in Table S2).

III.H. dc Magnetic Measurements. The temperature dependence of the dc magnetic susceptibility was measured on a powder sample of **I** in the temperature range 2–300 K with an applied magnetic field of 0.1 T. The results of these measurements are presented in Figure 8. The field dependences of the magnetization measured at $T = 2, 3, 4, 5, 7, 10$ K are shown in the inset in Figure 8.

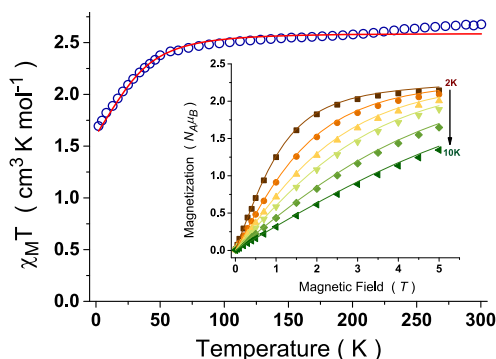


Figure 8. Temperature dependence of $\chi_M T$ for powder sample **I** measured at $B = 0.1$ T (dark blue open circles). Inset: the magnetization vs magnetic field for **I** measured at $T = 2, 3, 4, 5, 7, 10$ K (closed symbols). Theoretical curves (solid lines) are calculated with the parameters of the spin Hamiltonian eq 1, obtained above from EPR spectroscopic data: $D = 37.13 \text{ cm}^{-1}$, $\eta = 0.158$, $g_x = 2.388$, $g_y = 2.417$, and $g_z = 2.221$.

At room temperature $\chi_M T$ is found to be $\sim 2.677 \text{ cm}^3 \text{ K mol}^{-1}$, which is considerably higher than the spin-only value ($1.875 \text{ cm}^3 \text{ K mol}^{-1}$) because of considerable orbital contribution to the magnetic moment. This value falls within the range of typical values found in other quasi-octahedral high-spin Co(II) complexes.^{36–44,47} Upon cooling, the value of $\chi_M T$ gradually decreases in the temperature range from 300 K to around 70 K, and then it decreases sharply to reach a value of $\sim 1.694 \text{ cm}^3 \text{ K mol}^{-1}$ at 2 K. This sharp decrease in $\chi_M T$ can be attributed to a strong ZFS in **I**.

At $T = 2$ K the magnetization as a function of the magnetic field almost saturates at 5 T, reaching a value of around $2.16 N_A \mu_B$ (Figure 8), which is significantly lower than the value of $3 N_A \mu_B$, corresponding to the pure spin $S = 3/2$ with $g = 2.03$, but agrees well with the X-band EPR data obtained from the effective pseudo spin 1/2 ground Kramers doublet with $g_{\text{iso}} = 3.84$ (note that at $T = 2$ K only the population of this ground Kramers doublet is not negligible).

The theoretical curves calculated with the set of spin Hamiltonian parameters found from the proposed combined

spectroscopic approach are also shown in Figure 8. It is seen that both the calculated temperature dependence of $\chi_M T$ and the field dependences of magnetization are in satisfying agreement with the experimental magnetic data. Hence, this exemplifies the power of the proposed spectroscopic approach for the reliable determination of the spin Hamiltonian parameters of the Co(II) complexes.

IV. CONCLUSIONS

The accurate determination of the spin Hamiltonian parameters for high-spin transition metal complexes with large ZFS is an actual challenge for molecular spectroscopy. Unfortunately, there is no one unique approach to solve the problem. In the present study, we proposed a new combined experimental methodology based on EPR techniques in different frequency ranges for determination of the spin 3/2 Hamiltonian parameters and successfully applied this methodology to the new high-spin Co(II) complex I.

First, the principal values of the effective g' tensor for the effective pseudo spin 1/2 Hamiltonian related to the ground Kramers doublet were obtained by X-band and MHF EPR spectroscopy with high accuracy. Then the splitting between two Kramers doublets Δ was directly measured by the FD-FT THz-EPR technique. However, two components are missing to get the set of the spin 3/2 Hamiltonian parameters: the correct assignment of canonical resonance lines to the axes (x , y , z) and the value of $\eta = E/D$. In this work, we have demonstrated how to overcome these difficulties and to determine the full set of the spin 3/2 Hamiltonian parameters. The parameters for complex I obtained in this way are as follows: $g_x = 2.388(3)$, $g_y = 2.417(3)$, $g_z = 2.221(3)$, $\eta = 0.158(1)$, and $D = 37.1(5) \text{ cm}^{-1}$. The justification of the applicability of the spin Hamiltonian to the description of complex I was based on the results of multiconfigurational quantum-chemical calculations of the energy pattern of this complex.

The reliability of the obtained data is confirmed by perfect simulations of the experimental spectra for both the X-band EPR and the FD-FT THz EPR spectra. Furthermore, the SA-CASSCF/NEVPT2 quantum chemical calculations are in reasonable agreement with the experimental data and support all qualitative findings deduced from the experiments. Finally, the measured dc magnetic data are in satisfying agreement described by the set of spin Hamiltonian parameters derived from the EPR data without any fitting procedures.

Note that none of the used experimental technologies are new. The new aspect of this work is the combination of these three techniques and their analysis. The proposed method is not strict and universal. However, in practice, it should be applicable for a wide range of systems. While we have demonstrated here that it can be applied to quasi-octahedral Co(II) complexes, we expect it to be useful for all complexes with strongly anisotropic transition metal ions with $S = 3/2$, provided that the spin Hamiltonian formalism is applicable.⁸⁵ This explicitly includes Co(II) in different coordination geometries.

■ ASSOCIATED CONTENT

Supporting Information

The Supporting Information is available free of charge at <https://pubs.acs.org/doi/10.1021/acs.inorgchem.9b02195>.

Details of the synthesis and characterization of I and II, description of the Griffith Hamiltonian, orientation of the magnetic tensors calculated by CASSCF/NEVPT2, additional X-band, MHF-EPR, and FD-FT THz-EPR spectra, and further details on obtaining the magnetic parameters of I (PDF)

Accession Codes

CCDC 1911055 contains the supplementary crystallographic data for this paper. These data can be obtained free of charge via www.ccdc.cam.ac.uk/data_request/cif, or by emailing data_request@ccdc.cam.ac.uk, or by contacting The Cambridge Crystallographic Data Centre, 12 Union Road, Cambridge CB2 1EZ, UK; fax: +44 1223 336033.

■ AUTHOR INFORMATION

Corresponding Authors

*E-mail for E.Ya.M.: misochko@icp.ac.ru.

*E-mail for J.N.: joscha.nehrkorn@cec.mpg.de.

ORCID

Eugenii Ya. Misochko: 0000-0001-7903-8949

Denis V. Korchagin: 0000-0002-0199-1382

Joscha Nehrkorn: 0000-0003-1156-5675

Juan Modesto Clemente-Juan: 0000-0002-3198-073X

Notes

The authors declare no competing financial interest.

■ ACKNOWLEDGMENTS

A.V.A., D.V.K., A.V.P., J.M.C.-J., and S.M.A. acknowledge support from the Ministry of Science and Higher Education of the Russian Federation (Agreement No. 14.W03.31.0001-Institute of Problems of Chemical Physics, Chernogolovka). E.Ya.M. acknowledges the state assignment of the Ministry of Science and Higher Education of the Russian Federation (No. 0089-2019-0011). The National High Magnetic Field Laboratory is supported by the National Science Foundation through NSF/DMR-1644779 and the State of Florida. J.M.C.-J. thanks the Spanish MINECO (CTQ2017-89528-P) and Unit of Excellence María de Maeztu, MDM-2015-0538. The authors thank J. M. Martínez-Agudo from the Universidad de Valencia for the SQUID measurements and N.E. Kochetov from Moscow State University for help with X-band EPR.

■ REFERENCES

- (1) Winpenny, R. E. P. Quantum Information Processing Using Molecular Nanomagnets as Qubits. *Angew. Chem., Int. Ed.* **2008**, *47*, 7992–7994.
- (2) Gatteschi, D.; Cornia, A.; Mannini, M.; Sessoli, R. Organizing and Addressing Magnetic Molecules. *Inorg. Chem.* **2009**, *48* (8), 3408–3419.
- (3) Murrie, M. Cobalt(II) Single-Molecule Magnets. *Chem. Soc. Rev.* **2010**, *39* (6), 1986–1995.
- (4) Layfield, R. A. Organometallic Single-Molecule Magnets. *Organometallics* **2014**, *33*, 1084.
- (5) Gomez-Coca, S.; Urtizberea, A.; Cremades, E.; Alonso, P. J.; Camon, A.; Ruiz, E.; Luis, F. Origin of Slow Magnetic Relaxation in Kramers Ions with Non-Uniaxial Anisotropy. *Nat. Commun.* **2014**, *5* (1), 4300.
- (6) Benelli, C.; Gatteschi, D. Introduction to Molecular Magnetism: From Transition Metals to Lanthanides. *Introduction to Molecular Magnetism: From Transition Metals to Lanthanides* **2015**, 1–450.
- (7) Atanasov, M.; Aravena, D.; Suturina, E.; Bill, E.; Maganas, D.; Neese, F. First Principles Approach to the Electronic Structure, Magnetic Anisotropy and Spin Relaxation in Mononuclear 3d-

Transition Metal Single Molecule Magnets. *Coord. Chem. Rev.* **2015**, *289* (SI), 177–214.

(8) Krzystek, J.; Telser, J. Measuring Giant Anisotropy in Paramagnetic Transition Metal Complexes with Relevance to Single-Ion Magnetism. *Dalton Trans.* **2016**, *45* (42), 16751–16763.

(9) Craig, G. A.; Murrie, M. 3d Single-Ion Magnets. *Chem. Soc. Rev.* **2015**, *44* (8), 2135–2147.

(10) Boča, R. Zero-Field Splitting in Metal Complexes. *Coord. Chem. Rev.* **2004**, *248* (9–10), 757–815.

(11) Krzystek, J.; Ozarowski, A.; Telser, J. Multi-Frequency, High-Field EPR as a Powerful Tool to Accurately Determine Zero-Field Splitting in High-Spin Transition Metal Coordination Complexes. *Coord. Chem. Rev.* **2006**, *250*, 2308–2324.

(12) Yamane, T.; Sugisaki, K.; Matsuoka, H.; Sato, K.; Toyota, K.; Shiomi, D.; Takui, T. ESR Analyses of Picket Fence Mn II and 6th Ligand Coordinated Fe III Porphyrins ($S = 5/2$) and a Co II (hfac) Complex ($S = 3/2$) with Sizable ZFS Parameters Revisited: A Full Spin Hamiltonian Approach and Quantum Chemical Calculations. *Dalton Trans.* **2018**, *47*, 16429–16444.

(13) Suturina, E. A.; Nehr Korn, J.; Zdrozny, J. M.; Liu, J.; Atanasov, M.; Weyhermüller, T.; Maganas, D.; Hill, S.; Schnegg, A.; Bill, E.; et al. Magneto-Structural Correlations in Pseudotetrahedral Forms of the $[\text{Co}(\text{SPh})_4]^{2-}$ Complex Probed by Magnetometry, MCD Spectroscopy, Advanced EPR Techniques, and Ab Initio Electronic Structure Calculations. *Inorg. Chem.* **2017**, *56* (5), 3102–3118.

(14) Palić, A. V.; Korchagin, D. V.; Yureva, E. A.; Akimov, A. V.; Misochko, E. Y.; Shilov, G. V.; Talantsev, A. D.; Morgunov, R. B.; Aldoshin, S. M.; Tsukerblat, B. S. Single-Ion Magnet $\text{Et}_4\text{N}[\text{Co}^{\text{II}}(\text{hfac})_3]$ with Nonuniaxial Anisotropy: Synthesis, Experimental Characterization, and Theoretical Modeling. *Inorg. Chem.* **2016**, *55* (19), 9696–9706.

(15) Świtlicka, A.; Palion-Gazda, J.; Machura, B.; Cano, J.; Lloret, F.; Julve, M. Field-induced slow magnetic relaxation in pseudooctahedral cobalt(II) complexes with positive axial and large rhombic anisotropy. *Dalton Trans.* **2019**, *48*, 1404–1417.

(16) Tripathi, S.; Dey, A.; Shanmugam, M.; Narayanan, R. S.; Chandrasekhar, V. Cobalt(II) Complexes as Single-Ion Magnets. *Top. Organomet. Chem.* **2018**, 1–41.

(17) Liu, J. J.; Meng, Y. S.; Hlavička, I.; Orlita, M.; Jiang, S. Da; Wang, B. W.; Gao, S. Determination of Zero-Field Splitting in Co^{2+} Halide Complexes with Magnetic and Far-IR Measurements. *Dalton Trans.* **2017**, *46* (23), 7408–7411.

(18) Novitchi, G.; Jiang, S.; Shova, S.; Rida, F.; Hlavička, I.; Orlita, M.; Wernsdorfer, W.; Hamze, R.; Martins, C.; Suaud, N.; et al. From Positive to Negative Zero-Field Splitting in a Series of Strongly Magnetically Anisotropic Mononuclear Metal Complexes. *Inorg. Chem.* **2017**, *56* (24), 14809–14822.

(19) Rechkemmer, Y.; Breitgoff, F. D.; van der Meer, M.; Atanasov, M.; Hakl, M.; Orlita, M.; Neugebauer, P.; Neese, F.; Sarkar, B.; van Slageren, J. A Four-Coordinate Cobalt(II) Single-Ion Magnet with Coercivity and a Very High Energy Barrier. *Nat. Commun.* **2016**, *7*.

(20) Šebová, M.; Boča, R.; Dlháň, L.; Nemeč, I.; Papánková, B.; Pavlík, J.; Fuess, H. Direct Determination of Zero-Field Splitting in $\text{Co}(\text{II})$ Complexes by FAR Infrared Spectroscopy. *Inorg. Chim. Acta* **2012**, *383*, 143–151.

(21) Yao, X. N.; Du, J. Z.; Zhang, Y. Q.; Leng, X. B.; Yang, M. W.; Jiang, S. Da; Wang, Z. X.; Ouyang, Z. W.; Deng, L.; Wang, B. W.; et al. Two-Coordinate $\text{Co}(\text{II})$ Imido Complexes as Outstanding Single-Molecule Magnets. *J. Am. Chem. Soc.* **2017**, *139* (1), 373–380.

(22) Zdrozny, J. M.; Telser, J.; Long, J. R. Slow Magnetic Relaxation in the Tetrahedral Cobalt(II) Complexes $[\text{Co}(\text{EPh})_4]^{2-}$ ($\text{E} = \text{O}, \text{S}, \text{Se}$). *Polyhedron* **2013**, *64* (SI), 209–217.

(23) Barra, A. L.; Gatteschi, D.; Sessoli, R.; Abbati, G. L.; Cornia, A.; Fabretti, A. C.; Uytterhoeven, M. G. Electronic Structure of Manganese(III) Compounds from High-Frequency EPR Spectra. *Angew. Chem., Int. Ed. Engl.* **1997**, *36* (21), 2329–2331.

(24) Lynch, W. B.; Boorse, R. S.; Freed, J. H. A 250-GHz ESR Study of Highly Distorted Manganese Complexes. *J. Am. Chem. Soc.* **1993**, *115* (23), 10909–10915.

(25) Joyce, R. R.; Richards, P. L. Far-Infrared Spectra of Al_2O_3 Doped with Ti, V, and Cr. *Phys. Rev.* **1969**, *179* (2), 375–380.

(26) Brackett, G. C.; Richards, P. L.; Caughey, W. S. Far-Infrared Magnetic Resonance in $\text{Fe}(\text{III})$ and $\text{Mn}(\text{III})$ Porphyrins, Myoglobin, Hemoglobin, Ferrichrome A, and $\text{Fe}(\text{III})$ Dithiocarbamates. *J. Chem. Phys.* **1971**, *54* (10), 4383–4401.

(27) Champion, P. M.; Sievers, A. J. Far Infrared Magnetic Resonance in $\text{FeSiF}_6 \cdot 6\text{H}_2\text{O}$ and $\text{Fe}(\text{SPh})_4 \cdot 2\text{H}_2\text{O}$. *J. Chem. Phys.* **1977**, *66* (5), 1819–1825.

(28) Van Slageren, J.; Vongtragool, S.; Gorshunov, B.; Mukhin, A. A.; Karl, N.; Krzystek, J.; Telser, J.; Müller, A.; Sangregorio, C.; Gatteschi, D. Frequency-Domain Magnetic Resonance Spectroscopy of Molecular Magnetic Materials. *Phys. Chem. Chem. Phys.* **2003**, *5*, 3837–3843.

(29) Van der Put, P. J.; Schilperoord, A. A. Spin Delocalization in Square-Planar Spin-Triplet Benzene- and Toluenedithiolatecobaltate(III). *Inorg. Chem.* **1974**, *13* (10), 2476–2481.

(30) Ray, K.; Begum, A.; Weyhermüller, T.; Piligkos, S.; Van Slageren, J.; Neese, F.; Wieghardt, K. The Electronic Structure of the Isoelectronic, Square-Planar Complexes $[\text{Fe}(\text{L})_2]^{2-}$ and $[\text{Co}(\text{III})(\text{L Bu})_2]^{2-}$ (L_2^- and $(\text{L Bu})_2^- = \text{Benzene-1,2-Dithiolates}$): An Experimental and Density Functional Theoretical Study. *J. Am. Chem. Soc.* **2005**, *127* (12), 4403–4415.

(31) Telser, J.; Krzystek, J.; Ozarowski, A. High-Frequency and High-Field Electron Paramagnetic Resonance (HFEP): A New Spectroscopic Tool for Bioinorganic Chemistry. *JBIC, J. Biol. Inorg. Chem.* **2014**, *19*, 297–318.

(32) Schnegg, A.; Behrends, J.; Lips, K.; Bittl, R.; Holldack, K. Frequency Domain Fourier Transform THz-EPR on Single Molecule Magnets Using Coherent Synchrotron Radiation. *Phys. Chem. Chem. Phys.* **2009**, *11*, 6820–6825.

(33) Nehr Korn, J.; Veber, S. L.; Zhukas, L. A.; Novikov, V. V.; Nelyubina, Y. V.; Voloshin, Y. Z.; Holldack, K.; Stoll, S.; Schnegg, A. Determination of Large Zero-Field Splitting in High-Spin $\text{Co}(\text{I})$ Clathrochelates. *Inorg. Chem.* **2018**, *57* (24), 15330–15340.

(34) Pavlov, A. A.; Nehr Korn, J.; Pankratova, Y. A.; Ozerov, M.; Mikhalyova, E. A.; Polezhaev, A. V.; Nelyubina, Y. V.; Novikov, V. V. Detailed Electronic Structure of a High-Spin Cobalt(II) Complex Determined from NMR and THz-EPR Spectroscopy. *Phys. Chem. Chem. Phys.* **2019**, *21* (16), 8201–8204.

(35) Krzystek, J.; Kohl, G.; Hansen, H.-B.; Enders, M.; Telser, J. Combining HFEP and NMR Spectroscopies to Characterize Organochromium(III) Complexes with Large Zero-Field Splitting. *Organometallics* **2019**, *38* (9), 2179–2188.

(36) Serpthon, D.; Murray, K. S.; Phonsing, W.; Jover, J.; Ruiz, E.; Telfer, S. G.; Alkaş, A.; Harding, P.; Harding, D. J. Slow relaxation of magnetization in a bis-mer-tridentate octahedral $\text{Co}(\text{II})$ complex. *Dalton Trans.* **2018**, *47*, 859–867.

(37) Varga, F.; Rajnák, C.; Titiš, J.; Moncol, J.; Boča, R. Slow magnetic relaxation in a $\text{Co}(\text{II})$ octahedral–tetrahedral system formed of a $[\text{CoL}_3]^{2+}$ core with $\text{L} = \text{bis}(\text{diphenylphosphanoxy})\text{methane}$ and tetrahedral $[\text{CoBr}_4]^{2-}$ counter anions. *Dalton Trans.* **2017**, *46*, 4148–4151.

(38) Rajnák, C.; Titiš, J.; Moncol, J.; Renz, F.; Boča, R. Field-Supported Slow Magnetic Relaxation in Hexacoordinate $\text{Co}(\text{II})$ Complexes with Easy Plane Anisotropy. *Eur. J. Inorg. Chem.* **2017**, *2017*, 1520–1525.

(39) Roy, S.; Oyarzabal, I.; Vallejo, J.; Cano, J.; Colacio, E.; Bauza, A.; Frontera, A.; Kirillov, A. M.; Drew, M. G. B.; Das, S. Two Polymorphic Forms of a Six-Coordinate Mononuclear Cobalt(II) Complex with Easy-Plane Anisotropy: Structural Features, Theoretical Calculations, and Field-Induced Slow Relaxation of the Magnetization. *Inorg. Chem.* **2016**, *55*, 8502–8513.

(40) Váhovská, L.; Vitushkina, S.; Potočňák, I.; Trávníček, Z.; Herchel, R. Effect of linear and non-linear pseudohalides on the structural and magnetic properties of $\text{Co}(\text{II})$ hexacoordinate single-molecule magnets. *Dalton Trans.* **2018**, *47*, 1498–1512.

(41) Plenck, C.; Krause, J.; Rentschler, E. A Click-Functionalized Single-Molecule Magnet Based on Cobalt(II) and Its Analogous

Manganese(II) and Zinc(II) Compounds. *Eur. J. Inorg. Chem.* **2015**, 2015, 370–374.

(42) Tupolova, Yu. P.; Shcherbakov, I. N.; Popov, L. D.; Lebedev, V. E.; Tkachev, V. V.; Zakharov, K. V.; Vasiliev, A. N.; Korchagin, D. V.; Pali, A. V.; Aldoshin, S. M. Field-induced single-ion magnet behaviour of a hexacoordinated Co(II) complex with easy-axis-type magnetic anisotropy. *Dalton Trans.* **2019**, 48, 6960–6970.

(43) Zhu, Y.-Y.; Cui, C.; Zhang, Y.-Q.; Jia, J.-H.; Guo, X.; Gao, C.; Qian, K.; Jiang, S.-D.; Wang, B.-W.; Wang, Z.-M.; Gao, S. Zero-field slow magnetic relaxation from single Co(II) ion: a transition metal single-molecule magnet with high anisotropy barrier. *Chemical Science* **2013**, 4, 1802–1806.

(44) Peng, Y.; Bodenstern, T.; Fink, K.; Mereacre, V.; Anson, C. E.; Powell, A. K. Magnetic anisotropy of a CoII single ion magnet with distorted trigonal prismatic coordination: theory and experiment. *Phys. Chem. Chem. Phys.* **2016**, 18, 30135–30143.

(45) Novikov, V. V.; Pavlov, A. A.; Nelyubina, Y. V.; Boulon, M.-E.; Varzatskii, O. A.; Voloshin, Y. Z.; Winpenny, R. E. P. A Trigonal Prismatic Mononuclear Cobalt(II) Complex Showing Single-Molecule Magnet Behavior. *J. Am. Chem. Soc.* **2015**, 137, 9792–9795.

(46) Korchagin, D. V.; Shilov, G. V.; Aldoshin, S. M.; Morgunov, R. B.; Talantsev, A. D.; Yureva, E. A. Halogen Atom Effect on the Magnetic Anisotropy of Pseudotetrahedral Co(II) Complexes with a Quinoline Ligand. *Polyhedron* **2015**, 102, 147–151.

(47) Korchagin, D. V.; Pali, A. A. V.; Yureva, E. A.; Akimov, A. V.; Misochko, E. Y.; Shilov, G. V.; Talantsev, A. D.; Morgunov, R. B.; Shakin, A. A.; Aldoshin, S. M.; et al. Evidence of Field Induced Slow Magnetic Relaxation in: Cis-[Co(hfac)₂(H₂O)₂] Exhibiting Tri-Axial Anisotropy with a Negative Axial Component. *Dalton Trans.* **2017**, 46 (23), 7540–7548.

(48) Zadrozny, J. M.; Liu, J.; Piro, N. A.; Chang, C. J.; Hill, S.; Long, J. R. Slow Magnetic Relaxation in a Pseudotetrahedral Cobalt(II) Complex with Easy-Plane Anisotropy. *Chem. Commun.* **2012**, 48 (33), 3927–3929.

(49) *CrysAlis PRO, version 171.36.20*; Agilent Technologies UK Ltd: Yarnton, Oxfordshire, England, 2011.

(50) Sheldrick, G. M. *SHELXTL v.6.14, Structure Determination Software Suite*; Bruker AXS: Madison, WI, USA, 2000.

(51) Hassan, A.; Pardi, L.; Krzystek, J.; Sienkiewicz, A.; Goy, P.; Rohrer, M.; Brunel, L.-C. Ultrawide Band Multifrequency High-Field EMR Technique: A Methodology for Increasing Spectroscopic Information. *J. Magn. Reson.* **2000**, 142 (2), 300–312.

(52) Nehrkorn, J.; Holldack, K.; Bittl, R.; Schnegg, A. Recent Progress in Synchrotron-Based Frequency-Domain Fourier-Transform THz-EPR. *J. Magn. Reson.* **2017**, 280, 10–19.

(53) Stoll, S.; Schweiger, A. EasySpin, a Comprehensive Software Package for Spectral Simulation and Analysis in EPR. *J. Magn. Reson.* **2006**, 178 (1), 42–55.

(54) Nehrkorn, J.; Schnegg, A.; Holldack, K.; Stoll, S. General Magnetic Transition Dipole Moments for Electron Paramagnetic Resonance. *Phys. Rev. Lett.* **2015**, 114 (1), 010801.

(55) Nehrkorn, J.; Telsler, J.; Holldack, K.; Stoll, S.; Schnegg, A. Simulating Frequency-Domain Electron Paramagnetic Resonance: Bridging the Gap between Experiment and Magnetic Parameters for High-Spin Transition-Metal Ion Complexes. *J. Phys. Chem. B* **2015**, 119 (43), 13816–13824.

(56) Bain, G. A.; Berry, J. F. Diamagnetic Corrections and Pascal's Constants. *J. Chem. Educ.* **2008**, 85 (4), 532.

(57) Angeli, C.; Cimiraglia, R.; Evangelisti, S.; Leininger, T.; Malrieu, J. P. Introduction of N-Electron Valence States for Multireference Perturbation Theory. *J. Chem. Phys.* **2001**, 114 (23), 10252–10264.

(58) Angeli, C.; Cimiraglia, R.; Malrieu, J. P. N-Electron Valence State Perturbation Theory: A Fast Implementation of the Strongly Contracted Variant. *Chem. Phys. Lett.* **2001**, 350 (3–4), 297–305.

(59) Angeli, C.; Cimiraglia, R.; Malrieu, J. P. N-Electron Valence State Perturbation Theory: A Spinless Formulation and an Efficient Implementation of the Strongly Contracted and of the Partially Contracted Variants. *J. Chem. Phys.* **2002**, 117 (20), 9138–9153.

(60) Angeli, C.; Borini, S.; Cestari, M.; Cimiraglia, R. A Quasidegenerate Formulation of the Second Order N-Electron Valence State Perturbation Theory Approach. *J. Chem. Phys.* **2004**, 121 (9), 4043–4049.

(61) Angeli, C.; Bories, B.; Cavallini, A.; Cimiraglia, R. Third-Order Multireference Perturbation Theory: The n-Electron Valence State Perturbation-Theory Approach. *J. Chem. Phys.* **2006**, 124 (5), 054108. (62) Neese, F. The ORCA Program System. *WILEY Interdiscip. Rev. Mol. Sci.* **2012**, 2 (1), 73–78.

(63) Weigend, F.; Ahlrichs, R. Balanced Basis Sets of Split Valence, Triple Zeta Valence and Quadruple Zeta Valence Quality for H to Rn: Design and Assessment of Accuracy. *Phys. Chem. Chem. Phys.* **2005**, 7 (18), 3297–3305.

(64) Schäfer, A.; Horn, H.; Ahlrichs, R. Fully Optimized Contracted Gaussian Basis Sets for Atoms Li to Kr. *J. Chem. Phys.* **1992**, 97 (4), 2571–2577.

(65) Schäfer, A.; Huber, C.; Ahlrichs, R. Fully Optimized Contracted Gaussian Basis Sets of Triple Zeta Valence Quality for Atoms Li to Kr. *J. Chem. Phys.* **1994**, 100 (8), 5829–5835.

(66) Maurice, R.; Bastardis, R.; de Graaf, C.; Suaud, N.; Mallah, T.; Guihery, N. Universal Theoretical Approach to Extract Anisotropic Spin Hamiltonians. *J. Chem. Theory Comput.* **2009**, 5 (11), 2977–2984.

(67) Neese, F. Efficient and Accurate Approximations to the Molecular Spin-Orbit Coupling Operator and Their Use in Molecular g-Tensor Calculations. *J. Chem. Phys.* **2005**, 122 (3), 034107.

(68) Maganas, D.; Sottini, S.; Kyritsis, P.; Groenen, E. J. J.; Neese, F. Theoretical Analysis of the Spin Hamiltonian Parameters in (CoS₄)-S(II) Complexes, Using Density Functional Theory and Correlated Ab Initio Methods. *Inorg. Chem.* **2011**, 50 (18), 8741–8754.

(69) Atanasov, M.; Ganyushin, D.; Sivalingam, K.; Neese, F.; Mingos, D. M. P.; Day, P.; Dahl, J. P. Molecular Electronic Structures of Transition Metal Complexes II. *Struct. Bonding (Berlin, Ger.)* **2011**, 143, 149–220.

(70) Singh, S. K.; Eng, J.; Atanasov, M.; Neese, F. Covalency and Chemical Bonding in Transition Metal Complexes: An Ab Initio Based Ligand Field Perspective. *Coord. Chem. Rev.* **2017**, 344, 2–25.

(71) Grigor'ev, A. N.; Steblyanko, A. Yu.; Goncharov, A. V.; Potekhin, K. A.; Batsanov, A. S.; Struchkov, Yu. T. The Crystal Structure of Bis(acetylacetonato)(2,2'-dipyridyl)cobalt (II). *Zh. Neorg. Khim.* **1987**, 32, 706–709.

(72) Steblyanko, A. Yu.; Grigor'ev, A. N.; Martynenko, L. I.; Reshetnyak, M. V.; Batsanov, A. S.; Struchkov, Yu. T. About Polymorphism of Bis(acetylacetonato)(2,2'-dipyridyl)cobalt. *Zh. Neorg. Khim.* **1988**, 33, 1515–1517.

(73) Riblet, F.; Novitchi, G.; Scopelliti, R.; Helm, L.; Gulea, A.; Merbach, A. Isomerization Mechanisms of Stereolabiletris- and bis-Bidentate Octahedral Cobalt(II) Complexes: X-ray Structure and Variable Temperature and Pressure NMR Kinetic Investigations. *Inorg. Chem.* **2010**, 49, 4194–4211.

(74) Harding, P.; Harding, D. J.; Daengngern, R.; Thurakitsaree, T.; Schutte, B. M.; Shaw, M. J.; Tantirungrotechai, Y. Redox Coupled-Spin Crossover in Cobalt β -Diketonate Complexes: Structural, Electrochemical and Computational Studies. *Polyhedron* **2012**, 42, 291–301.

(75) Rajnák, C.; Titiš, J.; Moncol, J.; Renz, F.; Boča, R. Field-Supported Slow Magnetic Relaxation in Hexacoordinate Co^{II} Complexes with Easy Plane Anisotropy. *Eur. J. Inorg. Chem.* **2017**, 2017 (11), 1520–1525.

(76) Varga, F.; Rajnák, C.; Titiš, J.; Moncol, J.; Boča, R. Slow Magnetic Relaxation in a Co(II) Octahedral–Tetrahedral System Formed of a [CoL₃]²⁺ Core with L = Bis(Diphenylphosphanoxido) Methane and Tetrahedral [CoBr₄]²⁻ Counter Anions. *Dalt. Trans.* **2017**, 46 (13), 4148–4151.

(77) Mandal, S.; Mondal, S.; Rajnák, C.; Titiš, J.; Boča, R.; Mohanta, S. Syntheses, Crystal Structures and Magnetic Properties of Two Mixed-Valence Co(III)Co(II) Compounds Derived from Schiff Base Ligands: Field-Supported Single-Ion-Magnet Behavior with Easy-Plane Anisotropy. *Dalt. Trans.* **2017**, 46 (38), 13135–13144.

(78) Boča, R.; Rajnák, C.; Moncol, J.; Titiš, J.; Valigura, D. Breaking the Magic Border of One Second for Slow Magnetic Relaxation of Cobalt-Based Single Ion Magnets. *Inorg. Chem.* **2018**, *57* (22), 14314–14321.

(79) Rigamonti, L.; Bridonneau, N.; Poneti, G.; Tesi, L.; Sorace, L.; Pinkowicz, D.; Jover, J.; Ruiz, E.; Sessoli, R.; Cornia, A. A Pseudo-Octahedral Cobalt(II) Complex with Bispyrazolylpyridine Ligands Acting as a Zero-Field Single-Molecule Magnet with Easy Axis Anisotropy. *Chem. - Eur. J.* **2018**, *24* (35), 8857–8868.

(80) Piwowarska, D.; Gnutek, P.; Rudowicz, C. Origin of the Ground Kramers Doublets for $\text{Co}^{2+}(\text{3d}^7)$ Ions with the Effective Spin $3/2$ Versus the Fictitious 'Spin' $1/2$. *Appl. Magn. Reson.* **2019**, *50*, 797–808.

(81) Vaidya, S.; Shukla, P.; Tripathi, S.; Rivière, E.; Mallah, T.; Rajaraman, G.; Shanmugam, M. Substituted versus Naked Thiourea Ligand Containing Pseudotetrahedral Cobalt(II) Complexes: A Comparative Study on Its Magnetization Relaxation Dynamics Phenomenon. *Inorg. Chem.* **2018**, *57* (6), 3371–3386.

(82) Pardi, L. A.; Krzystek, J.; Telser, J.; Brunel, L. C. Multi-frequency EPR Spectra of Molecular Oxygen in Solid Air. *J. Magn. Reson.* **2000**, *146* (2), 375–378.

(83) Alonso, P. J.; Forniés, J.; García-Monforte, M. A.; Martín, A.; Menjón, B.; Rillo, C. Synthesis and Characterization of New Paramagnetic Tetraaryl Derivatives of Chromium and Molybdenum. *J. Organomet. Chem.* **2007**, *692* (15), 3236–3247.

(84) Bartolomé, E.; Alonso, P. J.; Arauzo, A.; Luzón, J.; Bartolomé, J.; Racles, C.; Turta, C. Magnetic Properties of the Seven-Coordinated Nanoporous Framework Material $\text{Co}(\text{bpy})_{1.5}(\text{NO}_3)_2$ (bpy = 4,4'-Bipyridine). *Dalton Trans.* **2012**, *41* (34), 10382–10389.

(85) The proposed method has been already tested on two tetrahedral Co(II) complexes, and its applicability was demonstrated. The results of this study are in preparation for publication.